POPULATION GENOMIC ANALYSIS OF *CRYPTOCOCCUS* BRAZILIAN ISOLATES REVEALS AN AFRICAN TYPE SUBCLADE DISTRIBUTION

Corinne MAUFRAIS[1,2†], Luciana de OLIVEIRA[1†], Rafael W. BASTOS[3], Frédérique MOYRAND[1], Flavia C. G. REIS[4,5], Clara VALERO[3], Bianca GIMENEZ[4], Luisa J. JOSEFOWICZ[4], Gustavo H. GOLDMAN[3], Marcio L. RODRIGUES[4,6] and Guilhem JANBON[1]*

[1] Institut Pasteur, Unité Biologie des ARN des Pathogènes Fongiques, Département de Mycologie, F-75015, Paris, France
[2] Institut Pasteur, HUB Bioinformatique et Biostatistique, C3BI, USR 3756 IP CNRS, F-75015, Paris, France
[3] Departamento de Ciências Farmacêuticas, Faculdade de Ciências Farmacêuticas de Ribeirão Preto, Universidade de São Paulo, Ribeirão Preto,Brazil
[4] Instituto Carlos Chagas, Fundação Oswaldo Cruz (FIOCRUZ), Curitiba, Brazil
[5] Centro de Desenvolvimento Tecnologico em Saude (CDTS-Fiocruz), Brazil
[6] Instituto de Microbiologia Paulo de Góes (IMPG), Universidade Federal do Rio de Janeiro, Rio de Janeiro, Brazil

* Corresponding author
[†] Both authors should be considered as first authors

Abstract

The genomes of a large number of *Cryptococcus neoformans* isolates have been sequenced and analyzed in recent years. These genomes have been used to understand the global population structure of this opportunistic pathogen. However, only a small number of South American isolates have been considered in these studies, and the population structure of *C. neoformans* in this part of the world remains elusive. Here, we analyzed the genomic sequences of 53 Brazilian *Cryptococcu*s isolates and deciphered the *C. neoformans* population structure in this country. Our data reveal an African-like structure that suggested repeated intercontinental transports from Africa to South America. We also identified a mutator phenotype in one VNBII Brazilian isolate, exemplifying how fast-evolving isolates can shape the *Cryptococcus* population structure. Finally, phenotypic analyses revealed wide diversity but not lineage specificity in the expression of classical virulence traits within the set of isolates.

40 The current classification identifies seven human-pathogenic *Cryptococcus* species,
41 which are responsible for 180,000 deaths every year in the world (Hagen *et al.* 2015;
42 Rajasingham *et al.* 2017). *C. neoformans* and *C. deneoformans* represent the *neoformans*
43 group of species, whereas the *gattii* group of species comprises *C. gattii*, *C. deuterogattii*, *C.*
44 *tetragattii*, *C. decagattii*, and *C. bacillisporus* (Hagen *et al.* 2015). *C. neoformans* is the most
45 common species in clinical settings, representing more than 95% of the clinical isolates (Kwon-
46 Chung *et al.* 2014; Janbon *et al.* 2019). This species affects mostly immunocompromised
47 patients in whom it provokes meningoencephalitis. Other species, such as *C. gattii*, can be
48 primary pathogens and cause pulmonary infections (Kwon-Chung *et al.* 2014). *C. neoformans* is
49 thought to be acquired very early in life and can stay in a dormant state for years, probably in
50 alveolar macrophages (Garcia-Hermoso *et al.* 1999; Alanio 2020). As soon as a defect in the
51 cellular immunity appears, yeast cells can multiply, reach the central nervous system, and
52 induce meningoencephalitis, which is invariably deadly if untreated.
53 *C. neoformans* strains are ubiquitous in the environment and have been isolated from all
54 continents except Antarctica. Similarly, although isolates of the *gattii* group of species have
55 been long considered to be geographically restricted to tropical and subtropical regions and
56 typically associated with *Eucalyptus* trees, they have emerged as a primary pathogen in
57 western Canada and the United States of America (Kidd *et al.* 2004). Both species can live in a
58 broad range of ecological habitats and have been commonly isolated from soil, guano,
59 decaying wood, fruits, and insects (Lin and Heitman 2006). Pigeons (*Columba livia*) are vectors
60 for the worldwide dissemination of *Cryptococcus*. Indeed, dry pigeon guano seems to be an
61 ideal environment for *C. neoformans* development and is commonly infected with this fungus.
62 Nevertheless, pigeons are usually not harmed by *C. neoformans* because their body
63 temperature is too high (42.5°C) for its growth and disease development (Johnston *et al.*
64 2016).

65 All *neoformans* and *gattii* species are haploid species with two possible mating type alleles
66 (*MAT***a** and *MATα*) and a bipolar mating system. Efficient sexual reproduction has also been
67 described in the laboratory. Nevertheless, *C. neoformans MAT***a** isolates are rare in clinical and
68 environmental isolates with the exception of some places in Africa (Kwon-Chung and Bennett
69 1978; Litvintseva *et al.* 2003). In addition, it has been reported that 8% of the population of *C.*
70 *neoformans* isolates are diploid (Lin *et al.* 2009). Diverse hybrids have also been isolated from
71 environmental and clinical sources. The most common are AD hybrids, which are produced by
72 hybridization of *C. neoformans* with *C. deneoformans* isolates. In addition, rare cases of
73 *gattii*/*neoformans* hybrids have been reported (Bovers *et al.* 2008; Aminnejad *et al.* 2012).
74 Nevertheless, population structure analysis suggested that the different *neoformans* and *gattii*
75 populations are largely clonal with a limited degree of recombination (Litvintseva *et al.* 2005;
76 Bui *et al.* 2008; Litvintseva and Mitchell 2012).
77 Historically, these analyses were based on serotyping, which was first replaced by PCR-based
78 characterization (RAPD, AFLP, mating type analysis) of the isolates and then by sequencing of a
79 defined set of genes by multilocus sequence typing (MLST) (Ruma *et al.* 1996; Boekhout *et al.*
80 2001; Matsumoto *et al.* 2007; Meyer *et al.* 2009a). Originally, five *neoformans* molecular
81 subtypes were thus defined (VNI, VNII, VNIV, VNIII, and VNB) (Meyer *et al.* 2009b). The new
82 species definition includes VNI, VNII, and VNB within *C. neoformans*, VNIV within *C.*
83 *deneoformans*, and VNIII as *C. neoformans*/*C. deneoformans* hybrids. VNI is the most common
84 *C. neoformans* molecular subtype and has a global distribution. The VNB subtype was discovered
85 in Africa and has a genetically variable population with 10% *MAT***a** isolates, which are very rare
86 in all other studied populations (Litvintseva *et al.* 2003). The VNB clade includes strains isolated
87 from the endemic mopane tree (*Colophospermum mopane*), whereas strains isolated from
88 pigeon excreta in the same area had the VNI molecular type, which is shared by most isolates
89 globally. This observation supported the "out of Africa" hypothesis in which few of these isolates

90 would have adapted their biology to multiply in pigeons to achieve global dispersion (Litvintseva
91 *et al.* 2011; Litvintseva and Mitchell 2012).
92 More recently, the improvement of sequencing technologies and bioinformatics tools allowed
93 analysis of whole genome sequences, revealing new details in the structure and global
94 geographical distribution of the *Cryptococcus* populations together with the identification of
95 additional clades and subclades (Farrer *et al.* 2019). Most of these studies focused on *C.*
96 *neoformans*, with >1000 *C. neoformans* genome sequences analyzed in four studies
97 (Desjardins *et al.* 2017; Rhodes *et al.* 2017b; Vanhove *et al.* 2017; Ashton *et al.* 2019; Ergin *et*
98 *al.* 2019). Through these efforts, the VNB clade has been separated into the VNBI and VNBII
99 subclades, which have different resistance to oxidative stress and a different ability to produce
100 melanin (Desjardins *et al.* 2017; Vanhove *et al.* 2017). The VNI clade has been separated into a
101 number of subclades with three phylogenetic groups representing the majority of the studied
102 isolates (Rhodes *et al.* 2017b; Ashton *et al.* 2019). Surprisingly, only 11 haploid strains isolated
103 in South America were included in these studies. This small number conflicts with the
104 relevance of South America as a source of genetic diversity in the *gattii* isolates (Engelthaler *et*
105 *al.* 2014). Up until now, the only analysis of *C. neoformans* population structure in South
106 America has been an MLST analysis that concluded that subtype ST93 was the most prevalent
107 among strains isolated from HIV patients in Southeastern Brazil with a low level of
108 recombination (Ferreira-Paim *et al.* 2017). Similarly, few phenotypic analyses that include
109 South American isolates have been published, and a recent analysis of virulence factor
110 expression within Brazilian *Cryptococcus* clinical isolates does not include any sequencing or
111 molecular typing analysis (De Sousa *et al.* 2020). In the present study, we analyzed the
112 phenotypes and genome sequences of 53 Brazilian isolates, revealing very high phenotypic
113 diversity within *Cryptococcus* isolates and a subclade distribution that suggests several waves
114 of *Cryptococcus* introduction from Africa to South America.
115

Material and Methods

Isolates used in this study

Strains 2B, 2C, 2D, 4C, 7, 33A1, 54A1, 56A1, 68B1, 69A1, 81A1, 96A1, 106A1, 144A1, 151A1, 176A1, 3Pb3, 5Pb2, 19Pb4, 23Pb2, 32Bp1, and RR 2605 were isolated from Northern Brazil (Dal Pupo *et al.* 2019) and kindly donated by Dr. Halan Dal Pupo. Strains Cn201, Cn359, Cn894, Cn14HC, and Cn201 were obtained from the culture collection of the Central Hospital of the University of São Paulo. All other isolates were obtained from the Collection of Pathogenic Fungi available at Fiocruz. No genomic information was available for any of these isolates before the present study.

Read alignment, variant detection, and ploidy analysis

Illumina reads were aligned to the *Cryptococcus* reference genomes using Minimap2 aligner v. 2.9 (Li 2018) with the "-ax sr" parameter. BAM files were sorted and indexed using SAMtools (Li *et al.* 2009) version 1.9. Picard version 2.8.1 (http://broadinstitute.github.io/picard) tools were used to identify duplicate reads and assign correct read groups to BAM files. SAMtools version 1.9 and Picard version 2.8.1 were then used to filter, sort, and convert SAM files and assign read groups and mark duplicate reads. Single-nucleotide polymorphisms (SNPs) and insertions/deletions (indels) were called using Genome Analysis Toolkit version 3.6 with ploidy=1 according to the GATK Best Practices. HaploScore parameters used to filter SNPs and indels included VariantFiltration, QD <2.0, LowQD, ReadPosRankSum<-8.0, LowRankSum, FS >60.0, HightFS, MQRankSum<-12.5, MQRankSum, MQ <40.0, LowMQ, and HaplotypeScore >13.0. Phyml version 20120412 (Guindon *et al.* 2010) with the GTR, NNIs substitution model was used to infer phylogenetic relationships between the isolates using the separate dataset of confident SNPs. To examine variations in ploidy across the genome, the sequencing depth at all positions was computed using SAMtools (Li *et al.* 2009), and then the average depth was computed for 1-kb windows across the genome.

MAT locus determination

144 The mating type of Brazilian isolates was determined as previously published (Rhodes *et al.*
145 2017b). Briefly, Illumina reads were aligned to the mating-type locus sequences [AF542529.2
146 and AF542528.2] using BWA-MEM. Computed average depths at the *SXI* and *STE20* loci using
147 SAMtools mpileup were used to determine the mating type.

148 **Population inference by fastSTRUCTURE**

149 We used fastStucture (Raj *et al.* 2014) to identify admixture in the dataset from K=2 to K=4.
150 After K=4, clusters with the highest number of isolates were split into sub-clusters, which likely
151 reflects an issue due to the number of isolates within clusters rather than true biological
152 significance.

153 **Drug susceptibility testing**

154 The minimum inhibitory concentration (MIC) of fluconazole (FLC) (Sigma-Aldrich) was
155 determined as described by M27-A3 (Institute 2017).

156 **Titan cell production**

157 Titan cell (TC) production was evaluated as described by Dambuza and colleagues with some
158 modifications (Dambuza *et al.* 2018). The isolates were cultivated in yeast peptone dextrose
159 (YPD) agar (1% yeast extract, 2% bacto-peptone, 2% glucose, 2% bacto-agar) for 48h at 30°C. A
160 single colony was transferred to 5 mL YNB without amino acids (Sigma Y1250) prepared
161 according to the manufacturer's instructions plus 2% glucose. After incubation overnight at 30°C
162 and 200 rpm, $1X10^3$ cells/mL were inoculated into 5 mL 1xPBS (phosphate buffer solution) + 10%
163 heat-inactivated (HI) fetal calf serum (FCS) and incubated for 72 h at 37°C, 5% CO_2. We visualized
164 the cells microscopically without any staining, and 50 cells were measured. TCs were considered
165 body cells (without the capsule) with a diameter >10 µm. The experiment was repeated twice.

166 **Capsule staining**

167 Fungal cells were cultivated in YPD agar for 24 h at room temperature. Single colonies were
168 transferred by sterile loop to the wells of a 96-well plate, each containing 200 µL of Roswell
169 Park Memorial Institute (RPMI) medium at a final cell density of 10^7 yeast/mL. The plates were

170 incubated for an additional 24 h at 37°C in 5% CO_2 and centrifuged to separate the cells from
171 the supernatants. The supernatants were stored for GXM analysis, and the cells were washed
172 twice in PBS for further fixation in 4% paraformaldehyde for 1 h at room temperature. Yeast
173 cells were then blocked (1% bovine serum albumin [BSA] in PBS for 1 h at 37°C) and incubated
174 with the 18B7 anti-GXM monoclonal antibody (Casadevall *et al.* 1992) (mAb 18B7; 10 μg/mL
175 for 1 h at 37°C), a kind gift from Dr. Arturo Casadevall (Johns Hopkins University). The cells
176 were washed and incubated with an Alexa Fluor 488-conjugated secondary antibody (10
177 μg/mL for 1 h at 37°C; Invitrogen, USA). The cells were finally stained with calcofluor white (5
178 μg/mL for 1 h at 37°C; Invitrogen, USA). Alternatively, the cells were counterstained with India
179 ink for capsular visualization. The cells were visualized on a Leica TCS SP5 confocal microscope
180 or analyzed with a FACS Canto II flow cytometer. Data were processed with the FACSDiva
181 software, version 6.1.3.

182 **Data availability**

183 All sequence data from this study have been submitted to GenBank under the BioProject
184 identification no. PRJNA702892.

185

186 **Results**

187 **Description of the origin of the Brazilian isolates**

188 We selected 53 *Cryptococcus* Brazilian isolates, of which 12 were classified as *C. gattii* and 41
189 as *C. neoformans.* More than 41% (n=22) were environmental isolates and 36% (n=19) were
190 clinical isolates. The origin of the isolate was unknown for the remaining 23% (n=12). Twenty-
191 one strains were isolated from pigeon excreta in Northern Brazil (Dal Pupo *et al.* 2019), 28
192 isolates were obtained from the culture collections available at Fiocruz, and 4 were acquired
193 from the Central Hospital of the University of São Paulo (Table S1).

194

195 **Genome characterization**

196 Whole genome sequencing was performed for each of the 53 Brazilian isolates considered in
197 this study. Between 2.7 and 10.9 million 100-nt paired-end reads were obtained and aligned to
198 eight *Cryptococcus* reference genomes using Minimap2 (Li 2018) (Table S1). Reference
199 genomes were *C. neoformans* strain H99 (Janbon *et al.* 2014), *C. deneoformans* strain JEC21
200 (Loftus *et al.* 2005; Gonzalez-Hilarion *et al.* 2016), *C. deuterogattii* strain R265 (Yadav *et al.*
201 2018; Gröhs Ferrareze *et al.* 2021), *C. gattii WM276*, *C. bacillisporus* strains CA1280 and
202 CA1873, *C. decagattiii* strain AFLP10, and *C. tetragattii* strain IND107 (Basenko *et al.* 2018). Of
203 the 53 isolates, 40 were identified as *C. neoformans* with >80% of the reads aligning to the H99
204 genome (<40% of reads could be aligned to any other reference genome). Among the 13
205 remaining isolates, 8 were *C. deuterogattii* and 5 were *C. gattii* (Table S1). Of note, we found
206 that isolate Cg366, which was previously identified as *C. gattii*, is actually a *C. neoformans*
207 isolate. Isolates Cn201 and Cn894, which were previously considered to be *C. neoformans*,
208 were identified as *C. deuterogattii* isolates.

209 In order to determine mating type, we compared the number of reads aligned to the *STE20a*,
210 *STE20alpha*, *SXI1*, and *SXI2* genes of the corresponding species. These analyses revealed that

211 all isolates were *MATα*, confirming the overwhelming dominance of this mating type in clinical
212 and environmental isolates observed in most areas in the world (Desjardins *et al.* 2017).
213 The analysis of the read alignment profiles provided insight into possible large duplications or
214 aneuploidies. All *C. neoformans* isolates displayed an even alignment profile. This observation
215 together with the absence of heterozygous SNPs in our analysis suggested that these isolates
216 are either haploid or euploid homozygotes. However, we observed a duplication of the end of
217 the chromosome 1 in three isolates (Cn160, Cn161, and Cn186)) (left side in Figure 1). The
218 isolate Cn161 apparently had additional duplications within chromosome 8. Similar patterns
219 were observed in the eight *C. deuterogattii* isolates, with two isolates (Cn201 and Cn894)
220 displaying a duplication of a region located in chromosomes 8 and 13, respectively. In contrast,
221 all five *C. gattii* isolates displayed an even alignment profile, suggesting that all are haploid
222 (data not shown).

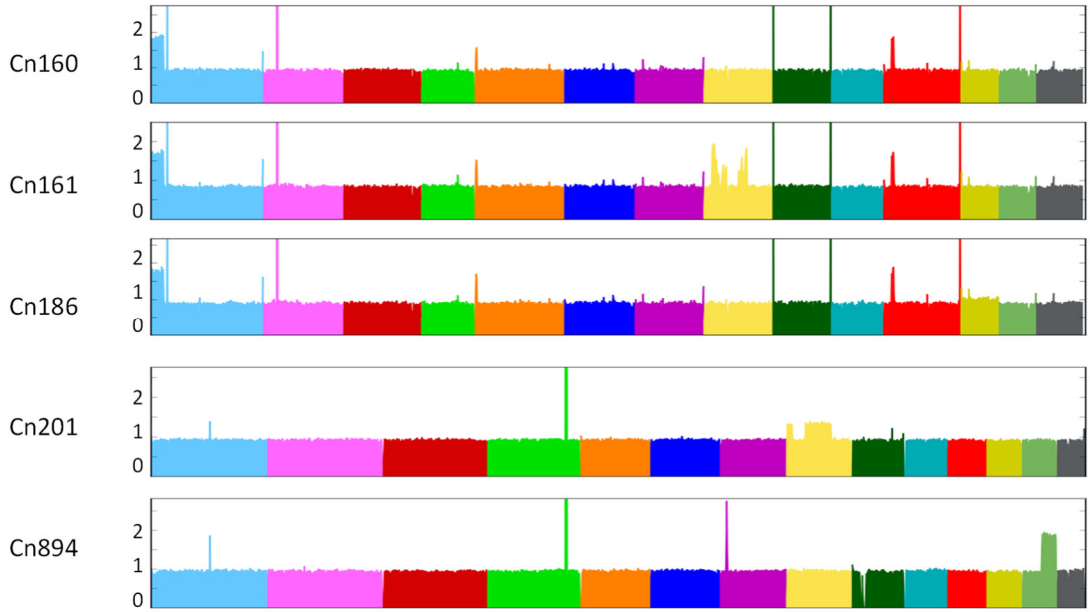

223

224 Figure 1. Large segmental duplications within the genomes of Brazilian isolates were revealed
225 after aligning sequencing reads to the *Cryptococcus* reference genomes.
226

227 **Phylogenetic analyses**

228 To obtain insight into the population structure of the Brazilian *C. neoformans* isolates, we
229 constructed a phylogenetic tree including 352 isolates considered in previous studies

230 (Desjardins *et al.* 2017; Rhodes *et al.* 2017b; Ashton *et al.* 2019) that encompass all VNI and
231 VNB subclades (Table S2). We also included 10 VNII isolates as the outgroup to root the tree
232 (Desjardins *et al.* 2017; Rhodes *et al.* 2017b; Ashton *et al.* 2019). Overall, 945,565 variable
233 positions were used to construct the tree presented in Figure 2A.
234
235 *VNB isolates*
236 Whereas the vast majority (92.5%, n=37) of the *C. neoformans* Brazilian isolates belonged to
237 the VNI clade, we also identified one VNB isolate of the VNBII subclade (Cn225). Two other
238 Brazilian isolates (Cn216 and Cn14HC) appear to be associated with the VNBI and VNBII clades,
239 respectively, but with a close-to-the-root long branch (Figure 2A). Accordingly, the number of
240 SNPs compared to the H99 reference genome was slightly higher in these two isolates than in
241 the other VNB isolates (Figure 2B). As previously reported, analysis of the population using
242 *fastSTRUCTURE* (k=4) (Raj *et al.* 2014) readily separated VNI, VNII, VNBI, and VNBII isolates
243 (Desjardins *et al.* 2017) into four independent populations (Figure 2C). As expected, this
244 analysis showed that the two Brazilian outlier isolates (Cn216 and Cn14HC) are associated with
245 the VNBI and VNBII clades, respectively.

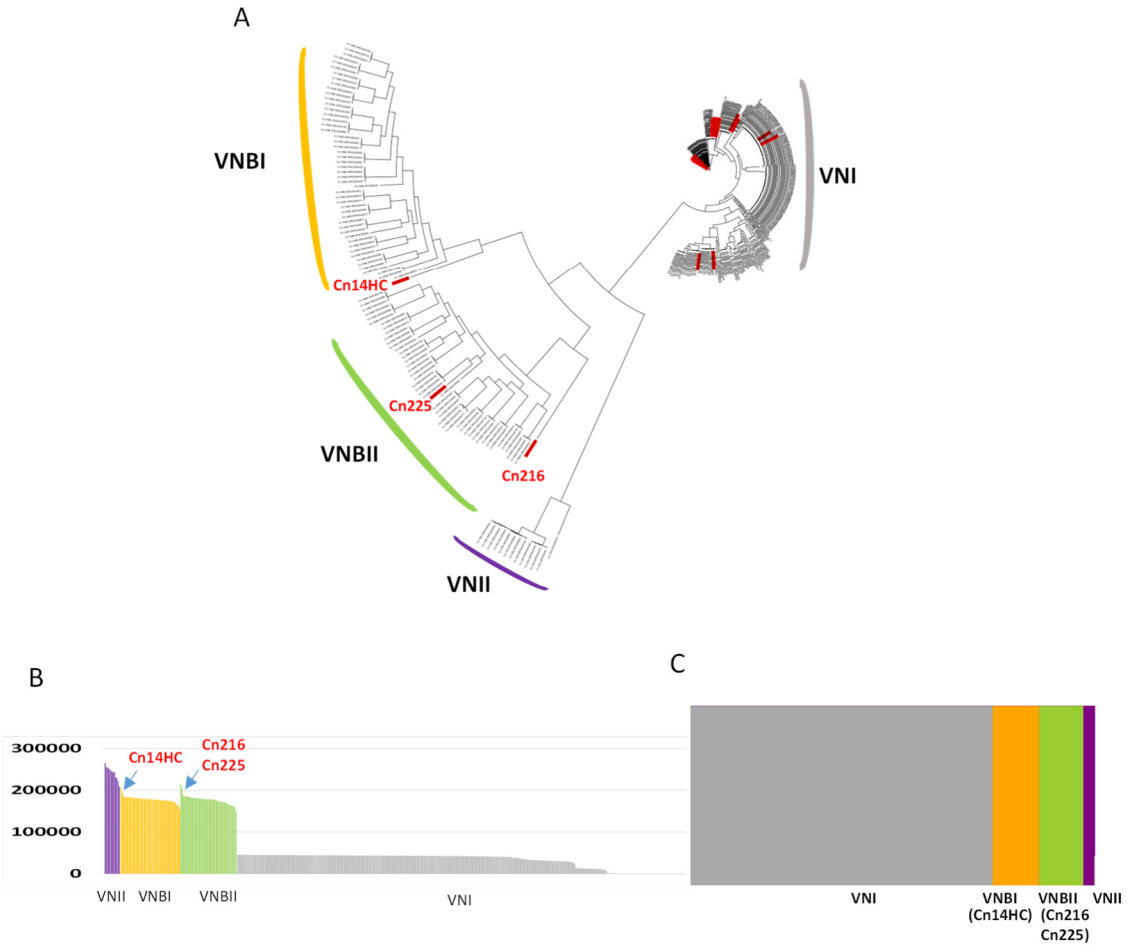

Figure 2. (A) Phylogenetic tree generated by iTOL v5 using *C. neoformans* genome sequences. The Brazilian isolates are indicated in red. The two Brazilian outlier isolates are shown. (B) Number of SNPs within the genomes of the different isolates analyzed in this study. (C) Results of the structure analysis (k=4) suggesting VNBI and VNBII origin for the two Brazilian outlier isolates (CnH14C and Cn216, respectively).

Because VNI/VNB and VNII/VNB hybrids have been previously reported within African isolates (Rhodes *et al.* 2017b), we sought to compare their phylogenetic position with the two outlier Brazilian isolates. We first redrew a phylogenetic tree including six of these isolates (the VNII/VNB isolate MW-RSA852 and four VNI/VNB isolates [Bt125, Bt131, Bt162, and Bt163]) (Figure S1). As previously published, the African hybrid isolates are also positioned at the root of the VNB and VNII branches, respectively. We then performed principal component analysis (PCA) including this set of hybrid isolates. As previously published, this analysis readily separated isolates positioned at an intermediary position between the defined clades (Figure

262 3) (Desjardins *et al.* 2017). Like most African VNI/VNB hybrids, the Bt163 isolate was

263 positioned between VNI and VNBII, suggesting that it is a hybrid of isolates of these two clades.

264 Of note, the VNI/VNB isolate Bt125 has an intermediary position between the VNBI, VNBII, and

265 VNI lineages (Figure 3).

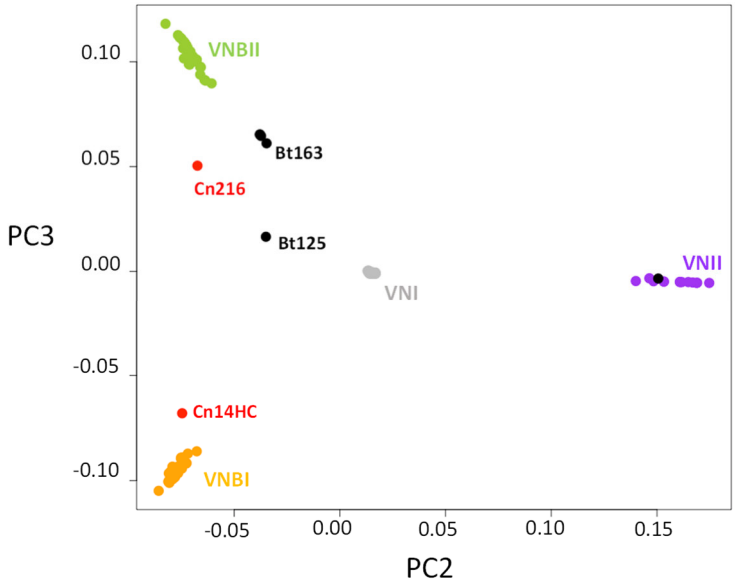

266

267 Figure 3. Principal component analysis revealing the intermediary position of the Brazilian
268 outlier isolates. VNI/VNB and VNII/VNB hybrid isolates (Rhodes *et al.* 2017b) have been added
269 to this analysis. The positions of the hybrid (black) and of the two Brazilian outlier isolates (in
270 red) are indicated.
271
272 The two outlier Brazilian isolates are positioned between the VNBI and VNBII isolates,

273 suggesting that they are not VNB/VNI hybrids. In agreement with the location of these isolates

274 in the phylogenetic tree, this analysis showed that the Cn216 isolate is closer to VNBII isolates

275 whereas the Cn14HC isolate is closer to VNBI isolates. According to these results, Cn216 and

276 CnH14C could be either VNBI/VNBII hybrids or evolved VNBI and VNBII isolates, respectively. In

277 order to test these two hypotheses, we first determined the position and number of SNPs

278 specific to each clade (Figure 4A,B). This analysis revealed that the number of clade-specific

279 SNPs was equivalent for each clade with an even distribution along the H99 reference genome.

280 Of note, the VNBI clade appear to have fewer clade-specific SNPs, which might be related to

281 the previously reported loss of diversity in this lineage (Desjardins *et al.* 2017).

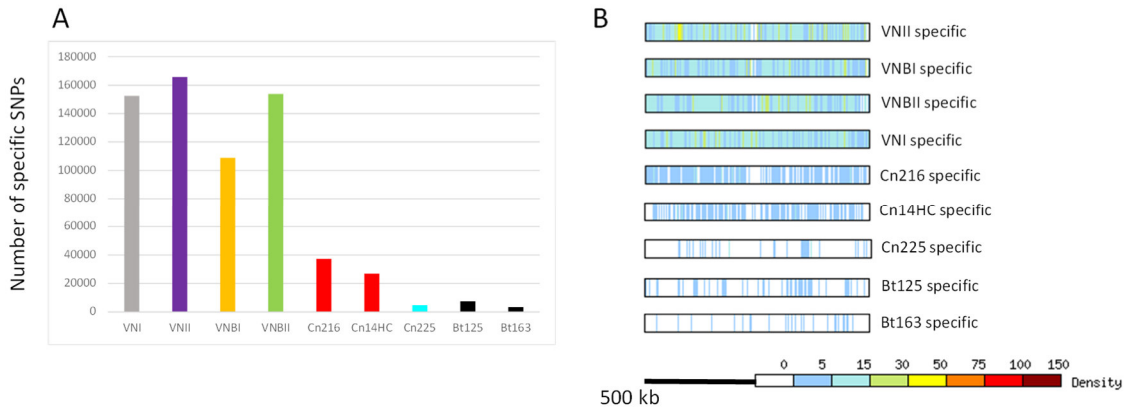

Figure 4. (A) Number of specific SNPs in each clade and in the two Brazilian outlier isolates (Cn216 and Cn14HC). The Brazilian VNBII isolate Cn225 and the hybrid isolates Bt125 and Bt163 (Rhodes *et al.* 2017b) were used as controls. (B) Density and position of the clade-specific SNPs in the H99 reference genome. The results obtained with chromosome 14 are presented.

We reasoned that we could determine the origins of the SNPs in the two outlier Brazilian isolates by comparing them with clade-specific SNPs (Figure 5). We compared the SNPs of Cn216 and Cn14HC SNPs (n=213,915 and n=207,438, respectively) with the VNI-, VNII-, VNBI-, and VNBI-specific SNPs and plotted their positions in the H99 reference genome. As a control, we performed the same analysis with the VNBII Brazilian isolate Cn215 (n=207,639 SNPs).

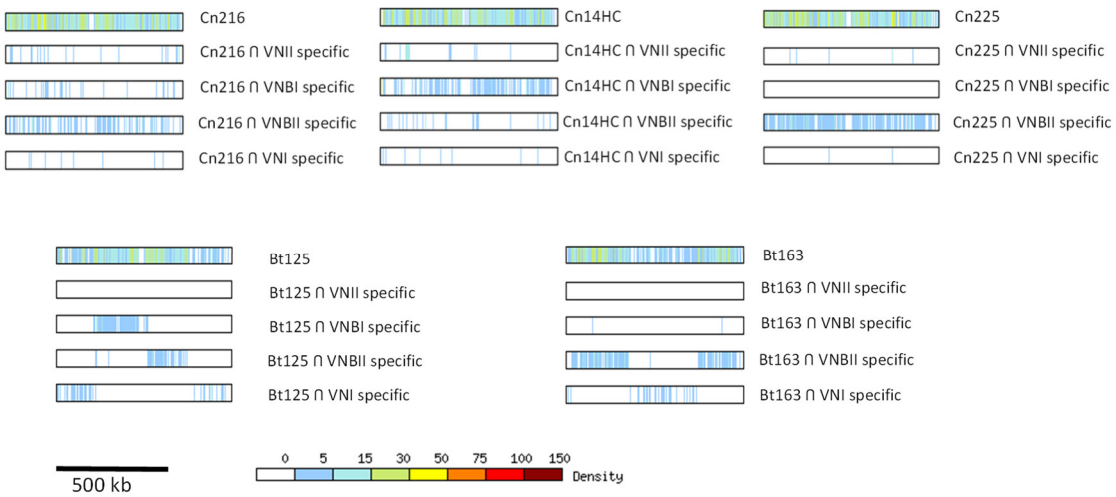

Figure 5. Origin of the SNPs in the Brazilian outlier isolates (Cn216 and Cn14HC). Positions of the SNPs shared between the clade-specific SNPs were identified and plotted on each chromosome. Chromosome 14 is presented as an example. Results obtained with the Brazilian VNBII Cn225 isolate and the African VNB/VNI hybrid isolates Bt125 and Bt163 (Rhodes *et al.* 2017b) are shown as controls.

301 This analysis revealed that the Brazilian outlier isolates Cn214 and Cn14HC mostly share SNPs
302 with the VNBII- and VNBI-specific SNPs, respectively, confirming that they belong to these
303 respective lineages. We observed an even distribution of these SNPs along the chromosomes
304 with no sign of a recent recombination event between the VNBI and VNBII lineages. As
305 expected, a similar result was obtained with the Brazilian VNBII isolate Cn225. In contrast, the
306 African VNB/VNI hybrid Bt163 displays a SNP distribution common to the clade-specific SNPs,
307 supporting a recent recombination event between a VNBII isolate and a VNI isolate and thus
308 confirming the PCA results and previously published results (Rhodes *et al.* 2017b). For the
309 Bt125 isolate, the SNP pattern was more complex than previously published, suggesting a
310 triple VNBI/VNBII/VNI origin for this isolate, in agreement with the intermediary position of
311 this isolate observed by PCA (Figure 3). Overall, these analyses suggest that the Cn214 and
312 CnH14C isolates belong to the VNBII and VNBI clades, respectively, with no sign of
313 recombination with another clade. Yet, the number of the SNPs unique to these two isolates
314 (n=37,236 in Cn216 and n=26,925 in CnH14C) is much higher than in the VNBII Brazilian isolate
315 Cn225 (n=4788) and in the two VNI/VNB African hybrids (n=7485 in Bt125 and n=3511 in
316 Bt163) (Figure 4A). These isolate-specific SNPs are evenly distributed along the H99 reference
317 genome (Figure 4B). This SNP pattern may be due to an ancient separation of these isolates
318 from most other isolates of their respective clades or a recent but rapid evolution of their
319 genome sequences due to an increased mutation rate.
320 In order to test these hypotheses, we compared the mutation rates in both Cn216 and Cn14HC
321 by observing the appearance of spontaneous 5-fluorouracil (FU)-resistant colonies in
322 fluctuation assays (Boyce *et al.* 2017; Billmyre *et al.* 2020). We included the reference strain
323 KN99α and the Brazilian VNBII isolate Cn225 as controls. The mutation rate of Cn14HC was
324 higher than those of Cn225 and KN99α (Figure 6). In contrast, the mutation rate in Cn216 was
325 not significantly different from that of Cn225 (VNBII). Similar results were obtained when 5-
326 FOA selection was used (Figure S2).

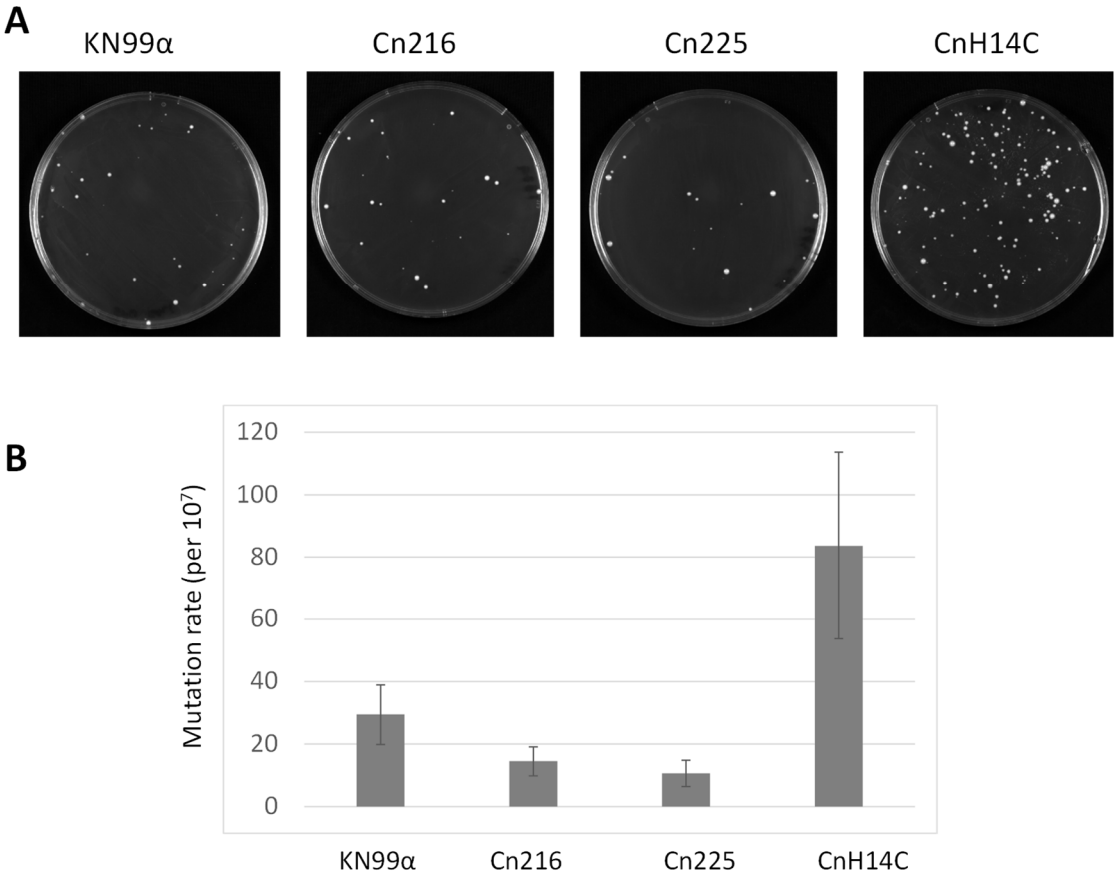

Figure 6. CnH14C display an elevated mutation rate. (A) Spontaneous 5-FU–resistant colonies in a standard wild type (KN99α) isolate and three Brazilian isolates (Cn216, Cn225, and CnH14C). (B) Quantitative assessment of mutation rates in the four strains using fluctuation analysis of the spontaneous resistance to 5-FU. The Lea-Coulson method of the median was used to estimate the number of mutations from the observed values of mutants from 10 independent, parallel cultures (Foster 2006; Gillet-Markowska *et al.* 2015). Error bars indicate 95% confidence intervals.

Isolates with mutations in the mismatch repair pathway associated with a mutator phenotype have been observed both in *C. deuterogattii* (Billmyre *et al.* 2017) and *C. neoformans* clinical isolates (Boyce *et al.* 2017; Rhodes *et al.* 2017a). Although experimental in vitro analyses suggested that only *MSH2*, *MLH1*, and *PMS1* play a major role in regulating the mutation rate in *C. neoformans* (Boyce *et al.* 2017), recurrent isolate evolution analysis suggested that *MSH5* and *RAD5* could also influence isolate evolution in patients (Rhodes *et al.* 2017a). Given that we did not identify Cn14HC nonsense mutations, we looked at the Cn14HC-specific SNPs responsible for non-conservative mutations in these mismatch repair genes. Interestingly, two

344 of these genes contain mutations specific to Cn14HC: *PMS1* (CNAG_07955) encodes a protein
345 with a S483P mutation and *RAD5* (CNAG_04733) encodes a protein with a P332S mutation.
346 These SNPs were not present in any of the other 391 isolates considered in this study. In
347 contrast, we did not identify specific SNPs responsible for a change in any of these proteins in
348 Cn216 or Cn225.
349 Overall, our results suggest that CnH14C possesses a mutator phenotype associated with
350 specific mutations in two mismatch repair genes. Of course, more experiments are needed to
351 formally establish a causal relationship between this genotype and this phenotype.
352 Nevertheless, the mutator phenotype of CnH14C has resulted in its rapid evolution, and could
353 explain its position in the phylogenic tree. In contrast, Cn216 might be the result of a long
354 evolution independent of the African VNBII isolate due to an ancient geographical separation.
355
356 *VNI isolates*
357 As stated above, nearly all *C. neoformans* isolates in this collection belong to the VNI clade,
358 mostly within the VNIa subclade. Only two isolates were identified as VNIb and none were
359 identified as VNIc. Interestingly, the second major lineage within the VNIa Brazilian isolates
360 was VNIa_Y, encompassing 27.5% (n=10) of isolates. All of these strains were isolated from
361 pigeon droppings in Northern Brazil. These are the first VNIa_Y strains isolated outside of
362 Africa; previous strains, all of which originated in the environment, were isolated in Botswana,
363 Malawi, and Uganda (Ashton *et al.* 2019). The population structure of the Brazilian VNIa
364 isolates resembles that of the African isolates. Approximately 45% of the VNIa isolates are of
365 the VNIa_93 lineage, similar to previous observations in Ugandan isolates (Ashton *et al.* 2019).
366 Similar to previous reports for African countries, only 2 of the Brazilian isolates were of the
367 VNIa_5 subclass and no VNIa_4 isolates were identified, confirming that these two subclasses
368 are specifically enriched within Southeast Asia isolates (Ashton *et al.* 2019).

369 Phylogenetic trees constructed using only the VNIa subclades revealed a clear geographical

370 clustering of the isolates (Figure 7), suggesting that the current subclade organization of *C.*

371 *neoformans* isolates predates the dissemination into South America. However, the existence of

372 unclustered VNI-93 Brazilian isolates suggests multiple intercontinental isolate transfers.

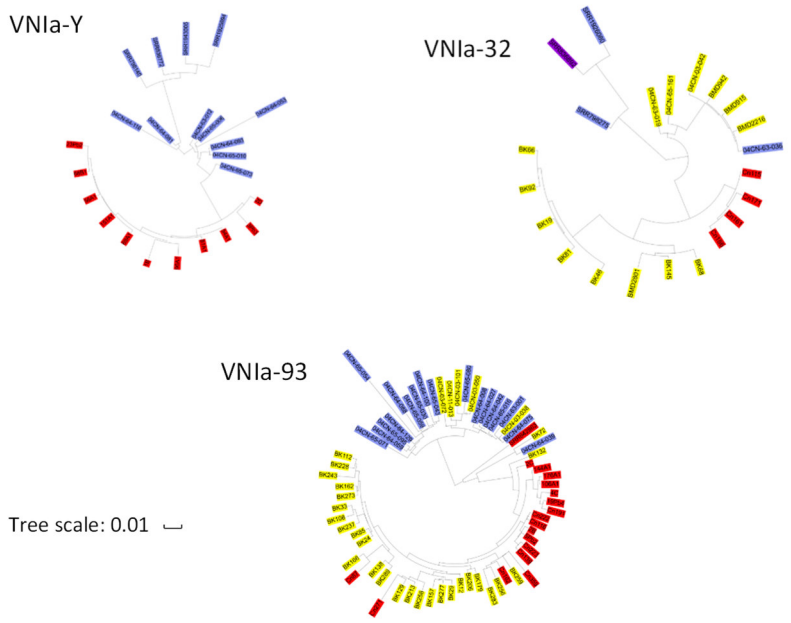

373

374 Figure 7. Phylogenetic trees of the VNIa subclades as visualized by ITOL revealed geographic
375 clustering. The Brazilian, African, and South Asian isolates are labelled in red, blue, and yellow,
376 respectively. The Indian isolates are labelled in purple.
377

378 **Phenotypic analyses**

379 We next characterized the Brazilian isolates at a phenotypic level. We focused our analysis on

380 virulence-associated phenotypes and drug resistance. All isolates grew well at 30°C, and only *C.*

381 *gattii* isolate Cg187 and *C. neoformans* VNIa_Y isolate 3Pb3 exhibited a growth defect at 37°C

382 (Figure S3). Similarly, most of these *Cryptococcus* isolates demonstrated a low MIC for

383 fluconazole (Table S3), with a MIC_{50} of 2 µg/mL and MIC_{90} of 8 µg/mL. The clinical isolate

384 Cn191 (VNIa_93) and the environmental isolate 151A1 (VNIa_Y) showed the highest MIC

385 values (8.0 µg/mL).

386 Capsule formation and exportation of GXM, a major capsular antigen, are essential for

387 *Cryptococcus* virulence. We analyzed multiple aspects of capsule formation in Brazilian

388 isolates, including capsular morphology, serological reactivity, and extracellular concentration
389 of GXM. Capsule morphology was examined by fluorescence microscopy after incubation of
390 the cells with an antibody to GXM for capsule visualization and calcofluor white for cell wall
391 staining. Alternatively, the capsule was counterstained with India ink for visualization of the
392 capsule by light microscopy. This analysis revealed formidable heterogeneity at morphological
393 and serological levels (Figure 8).

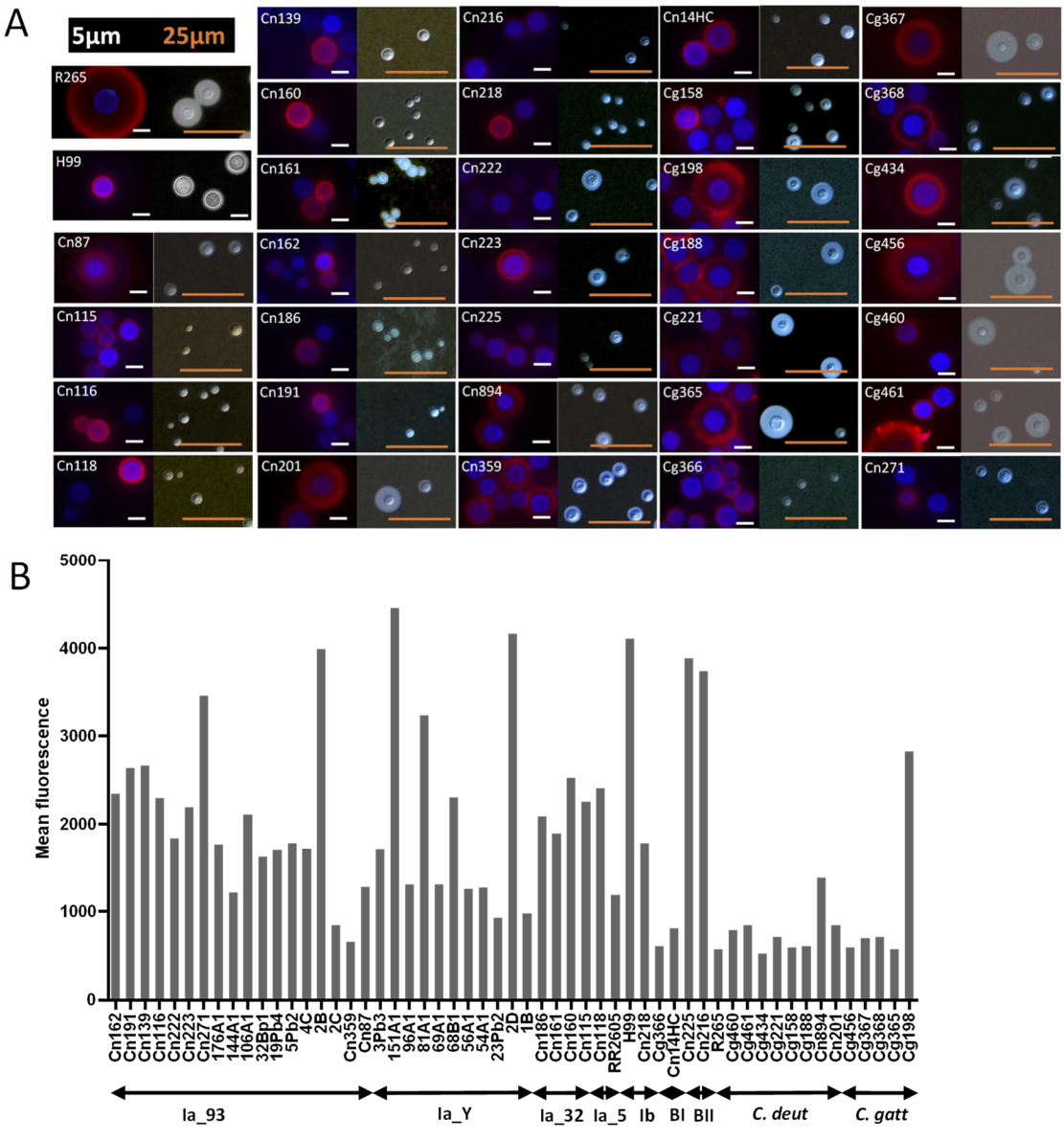

394

395 Figure 8 (A) Microscopic analysis of the cell surface of the Brazilian isolates. R265 and H99 are
396 standard cryptococcal isolates that were used as reference in this assay. For each isolate,
397 fluorescence panels are shown on the left and India ink counterstaining is shown on the right.
398 Red fluorescence indicates capsule staining with the mAb 18B7 antibody and blue fluorescence
399 represents cell wall staining. Images are illustrative of two independent analyses that

400 produced similar results. Corresponding data for the Northern Brazil isolates have been
401 previously published (Dal Pupo *et al.* 2019). (B) Flow cytometry analysis of the cryptococcal
402 isolates after capsule staining with mAb 18B7. At least 5000 cells were analyzed for each
403 isolate. Results are presented as average values of fluorescence intensity and are illustrative of
404 two independent analyses producing similar results. R265 and H99 are standard cryptococcal
405 isolates that were used as reference in this assay. Data for the Northern Brazil isolates were
406 obtained from (Dal Pupo *et al.* 2019).
407
408
409 On the basis of the visual perception that antibody recognition of the capsule was variable, we
410 measured the indices of fluorescence intensity after incubation of each isolate with the GXM-
411 binding antibody by flow cytometry (Figure 8B). Using the standard isolates H99 and R265 as
412 reference strains, this analysis confirmed both highly reactive isolates and poorly reactive
413 isolates, supporting the notion that surface GXM is highly diverse in *Cryptococcus*. Although *C.*
414 *gattii* and *C. deuterogattii* isolates were predominantly less capsulated than *C. neoformans*
415 (student t-test *P* value <0.05), we did not observe any statistical difference between the *C.*
416 *neoformans* subclades.
417 We also analyzed the concentration of polysaccharide in culture supernatants of each isolate
418 (Figure S4). Detection of extracellular and surface-associated GXM showed an apparent
419 correlation, as suggested by the statistical analysis (Figure S4), supporting the notion that
420 cryptococcal isolates are highly variable in their ability to form GXM-containing capsules and to
421 export polysaccharide.
422 We also examined melanin production on L-Dopa medium. We observed a variable phenotype
423 among the Brazilian isolates, with *C. gattii* and *C. deuterogattii* isolates displaying lower
424 melanin production (Figure 9). There was no obvious correlation between melanin production
425 among subclades, although strains isolated from bird droppings appear to produce more
426 melanin than other environmental or clinical isolates.

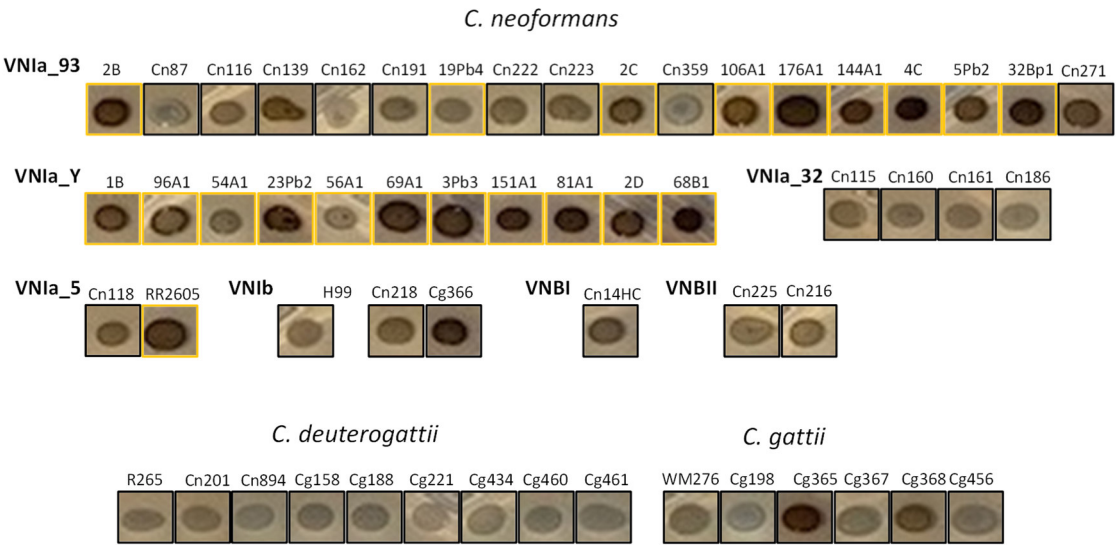

Figure 9. Melanin production of Brazilian isolates as estimated on L-Dopa medium after 72 h of incubation. Strains isolated from bird droppings are indicated by a yellow box.

Lastly, we examined production of TCs. *C. neoformans* and *C. gattii* cells can undergo an unusual transition in the host lung from the typical size of 5 to 7 µm to between 10 µm and 100 µm, a phenomenon known as titanization. TCs are known to be highly polyploid (Zaragoza and Nielsen 2013). TCs can also be induced in vitro using three different approaches (Dambuza *et al.* 2018; Hommel *et al.* 2018; Trevijano-Contador *et al.* 2018). Here, we followed the protocol described by Dambuza and colleagues (2018) to study whether Brazilian *Cryptococcus* isolates produce TCs. In our study, *C. neoformans* H99 formed nearly 17% TCs, aligning with previously published findings (Dambuza *et al.* 2018). Approximately 49% of Brazilian *Cryptococcus* isolates produced TCs (defined here as cells with a size >10 µm) (Figure 10, Table S4). Around 24% of Brazilian *Cryptococcus* isolates generated more TCs than *C. neoformans* H99 (Figure 10, Table S4). Interestingly, and in contrast to a previous study using the same protocol, all Brazilian *C. gattii* and *C. deuterogattii* isolates tested formed TCs (Figure 10, Table S4). The highest percentage of TCs (97.33%) was produced by *C. deuterogattii* isolate Cn894 (Figure 10, Table S4).

In order to address whether cells that formed more TCs than H99 are naturally larger, we compared the size of these cells before and after the titanization induction. The mean size of the cells of Brazilian *Cryptococcus* isolates varied between 4.18 to 5.70 µm before and 6.85

447 to 14.19 µm after cultivation in TC-inducing conditions, proving that the titanization induction

448 was responsible for the increase in cell size (Table S5). We did not observe any link between

449 subclade and the ability of the corresponding isolate to undergo this phenotypic change.

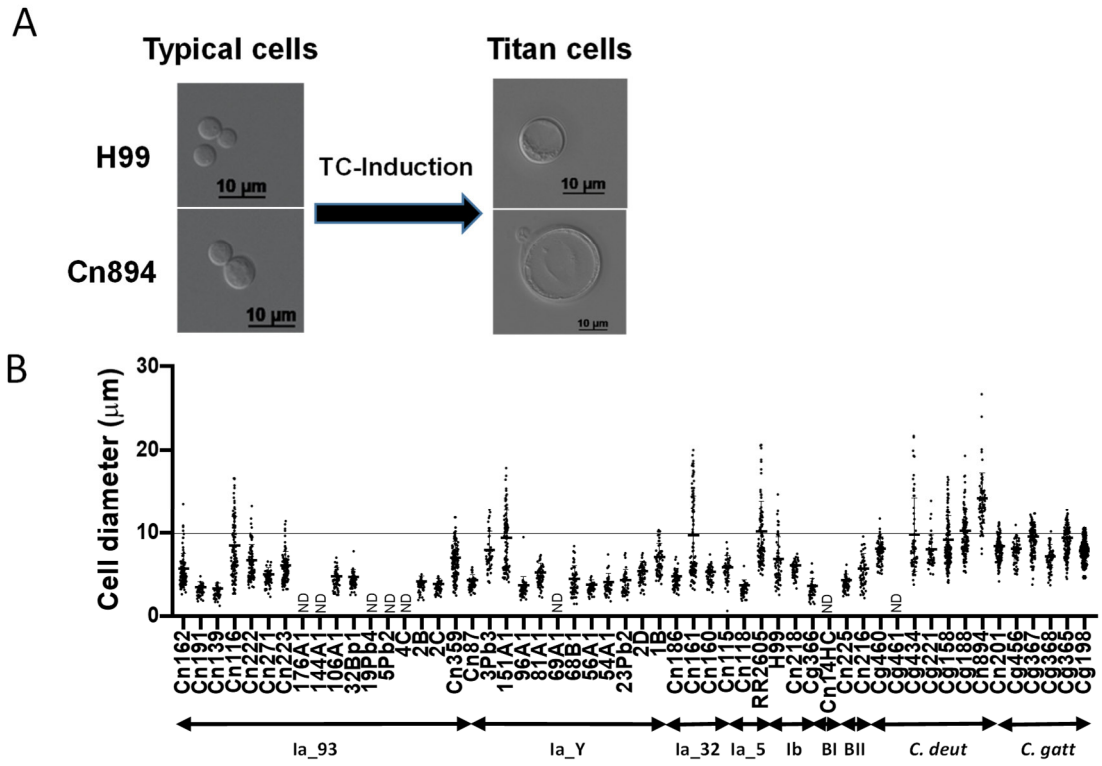

450

451 Figure 10. Cell diameter after titanization induction in Brazilian isolates. Cryptococcus isolates
452 were subjected to TC induction in PBS-HI-FCS. Cells with a diameter >10 µm were considered
453 to be TCs. ND: not determined.
454
455 Overall, this analysis revealed spectacular phenotypic variability within the Brazilian isolates,

456 although no association was detected between one clade and any of these phenotypic traits.

457

458 **Discussion**

459 Population genomics studies have resulted in a model in which clonal reproduction has shaped
460 the global population structure of *C. neoformans* isolates, which are mostly of the VNI clade
461 and of the *MATα* sexual type (Cuomo *et al.* 2018). These genome sequence analyses have also
462 identified several VNI subclades with specific geographical distribution (Ashton *et al.* 2019).
463 Currently, little is known about *Cryptococcus* species diversity in South America because only a
464 few isolates have been sequenced (Rhodes *et al.* 2017b). In the present study, we analyzed the
465 largest South American genome collection studied to date. As expected, most of the Brazilian
466 isolates belonged to the VNI clade. Our analysis revealed that the VNI Brazilian *C. neoformans*
467 population shares many features with the African population. For instance, VNI_Y isolates that
468 were previously reported only in Africa were also prominent within this set of South American
469 isolates. As in Africa, Brazilian VNIa_5 isolates were rare; in contrast, VNIa_5 isolates represent
470 one of the largest subclades within Asian isolates (Ashton *et al.* 2019). Actually, in most
471 regards, the *C. neoformans* Brazilian population structure is very different from the Asian one
472 described by Ashton and colleagues in 2019 (Ashton *et al.* 2019). A detailed analysis of the
473 different VNIa subclade population structures further supported the hypothesis of repeated
474 and privileged exchanges from African to South American isolates. Thus, South American
475 isolates do not form an independent clade or subclade but rather are scattered within nearly
476 all global subclades, indicating repeated transport. Although we observed a perfect clustering
477 of Brazilian isolates within the VNIa_Y and VNIa_32 subclades—possibly from an ancient
478 importation followed by independent evolution of the ancestral isolate—some VNIa-93
479 isolates clustered with the other global isolates, suggesting independent and possibly more
480 recent importations. Of course, because, all these unclustered VNI-93 Brazilian strains are
481 clinical isolates, we cannot completely exclude the hypothesis that these patients had travelled
482 to Africa, and had been infected there, before developing a cryptococcosis in Brazil as
483 previously described in some rare cases (Garcia-Hermoso *et al.* 1999).

484

485 A similar pattern was observed with the VNB isolates. Two of the Brazilian isolates were
486 positioned close to the roots of the VNB branches, as previously observed for two sequenced
487 Brazilian isolates (Rhodes *et al.* 2017b). However, the third isolate clustered within the other
488 VNB African isolates, suggesting a more recent intercontinental exchange. In that case, it is
489 important to note that this last strain has been isolated in the environment.
490 In 2017, Casadevall and colleagues suggested that the separation of *C. neoformans* complex
491 species and *C. gattii* complex species occurred in the middle of the Cretaceous period
492 (Casadevall *et al.* 2017). This geological period was marked by the breakup of the
493 supercontinent west Gondawa which encompassed Africa and South America. This modern
494 continent formation ended much before the global dispersion of major *Cryptococcus* spreader
495 birds (Prum *et al.* 2015) which occurred 40 x 10^6 years after the end of the Cretaceous period.
496 Although our data cannot reliably date the separation between the *C. neoformans* subclades,
497 the similar structure of the African and South American population suggests an African origin
498 for every *C. neoformans* isolates. In this model, the transport of *C. neoformans* from Africa to
499 South America started only with birds migrations 25 x 10^6 years ago and continued until today.
500 This study also exemplified the impact of rapidly evolving isolates on the *C. neoformans*
501 population structure. Mutator phenotypes have already been observed in natural *C.*
502 *neoformans* and *C. gattii* isolates and have been shown to impact the dynamics of isolate
503 evolution, phenotypic diversity, and drug resistance (Billmyre *et al.* 2017; Billmyre *et al.* 2020).
504 A *msh2*-associated mutator phenotype was also observed in a subset of *C. deuterogattii* Pacific
505 Northwest outbreak isolates, named VGIIa-like (Kidd *et al.* 2004; Billmyre *et al.* 2014; Billmyre
506 *et al.* 2017). Here, the VNBI isolate CnH14C displayed a mutator phenotype, albeit less
507 pronounced than the previously described *C. neoformans msh2Δ*, *mlh1Δ*, and *pms1Δ* mutant
508 strains (Boyce *et al.* 2017). Accordingly, we did not identify nonsense mutations in any of these
509 genes in the CnH14C isolate. However, *PMS1*- and *RAD5*-specific alleles in CnH14C might

510 suggest a causal relationship. In fact, *RAD5* has been recently identified as regulating mutation
511 rates in a quantitative trait locus analysis in *S. cerevisiae* (Gou *et al.* 2019), and a specific *RAD5*
512 mutation has also been identified in a rapidly evolved *C. neoformans* recurrent clinical isolate
513 (Rhodes *et al.* 2017a).
514 However, in contrast to what has been observed in some African isolates, we did not identify
515 any hybrid isolates within this collection of Brazilian isolates. As previously reported
516 (Matsumoto *et al.* 2007; Andrade-Silva *et al.* 2018), none of these isolates were *MAT***a**.
517 Nevertheless, our model of multiple intercontinental transport of African isolates to South
518 America and the proportion of *MAT***a** isolate within the VNB isolates in Africa (Litvintseva *et al.*
519 2007; Litvintseva *et al.* 2011; Litvintseva and Mitchell 2012) predict that additional sampling
520 will probably identify such isolates.
521 MLST and genome sequence analysis identified South America, and in particular Brazil, as the
522 major source of the global genetic diversity of the *C. gattii* complex, especially within the VGII
523 and VGIII lineages (Hagen *et al.* 2013; Billmyre *et al.* 2014; Souto *et al.* 2016; Barcellos *et al.*
524 2018; Vilas-Bôas *et al.* 2020). This is associated with great phenotypic diversity within the
525 Brazilian isolates (Silva *et al.* 2012; Barcellos *et al.* 2018). Similarly, genotypic and phenotypic
526 analyses of Brazilian *C. neoformans* isolates, including the analysis in the present study, have
527 revealed great diversity within South American isolates (Ferreira-Paim *et al.* 2017; Andrade-
528 Silva *et al.* 2018; Dal Pupo *et al.* 2019; De Sousa *et al.* 2020). Nevertheless, our data suggest
529 that Brazil is probably not an important source of global diversity of *C. neoformans* isolates.
530 Rather, our findings support the model in which this diversity is mostly imported from Africa
531 through repeated intercontinental transport of *C. neoformans* isolates to South America.
532 Our studies continue the investigation of *Cryptococcus* species global diversity and emphasize
533 the importance of understanding the evolution of fungal pathogens. Further studies with
534 additional isolates from Brazil and other countries in South America will help us to clarify many
535 aspects of population genetics of this important fungal pathogen.

Acknowledgments

M.L.R. is currently on leave from the position of associate professor at the Microbiology Institute of the Federal University of Rio de Janeiro, Brazil. M.L.R., G.J., and G.H.G. were supported by a Tripartite USP-Fiocruz-Pasteur grant. FCGR was financed in part by a scholarship from the Coordenação de Aperfeiçoamento de Pessoal de Nível Superior (CAPES, Brazil, Finance Code 001). This work in the Janbon lab was supported in part by an Infect-ERA grant (project Cryptoview).

544

545 References

546

547 Alanio, A., 2020 Dormancy in *Cryptococcus neoformans*: 60 years of accumulating
548 evidence. The Journal of Clinical Investigation 130**:** 3353-3360.
549 Aminnejad, M., M. Diaz, M. Arabatzis, E. Castaneda, M. Lazera *et al.*, 2012
550 Identification of novel hybrids between *Cryptococcus neoformans* var. *grubii*
551 VNI and *Cryptococcus gattii* VGII. Mycopathologia 173.
552 Andrade-Silva, L. E., K. Ferreira-Paim, T. B. Ferreira, A. Vilas-Boas, D. J. Mora *et al.*,
553 2018 Genotypic analysis of clinical and environmental *Cryptococcus*
554 *neoformans* isolates from Brazil reveals the presence of VNB isolates and a
555 correlation with biological factors. PLOS ONE 13**:** e0193237.
556 Ashton, P. M., L. T. Thanh, P. H. Trieu, D. Van Anh, N. M. Trinh *et al.*, 2019 Three
557 phylogenetic groups have driven the recent population expansion of
558 *Cryptococcus neoformans*. Nature Com. 10**:** 2035.
559 Barcellos, V. A., L. M. S. Martins, A. C. L. Fontes, J. C. V. Reuwsaat, E. D. Squizani *et al.*,
560 2018 Genotypic and phenotypic diversity of *Cryptococcus gattii* VGII Clinical
561 isolates and its Impact on Virulence. Frontiers in microbiology 9**:** 132-132.
562 Basenko, E. Y., J. A. Pulman, A. Shanmugasundram, O. S. Harb, K. Crouch *et al.*, 2018
563 FungiDB: An integrated bioinformatic resource for Fungi and Oomycetes. J.
564 Fungi 4**:** 39.
565 Billmyre, R. B., S. Applen Clancey, L. X. Li, T. L. Doering and J. Heitman, 2020 5-
566 fluorocytosine resistance is associated with hypermutation and alterations in
567 capsule biosynthesis in *Cryptococcus*. Nature Com. 11**:** 127.
568 Billmyre, R. B., S. A. Clancey and J. Heitman, 2017 Natural mismatch repair mutations
569 mediate phenotypic diversity and drug resistance in *Cryptococcus deuterogattii*.
570 eLife 6**:** e28802.
571 Billmyre, R. B., D. Croll, W. Li, P. Mieczkowski, D. A. Carter *et al.*, 2014 Highly
572 recombinant VGII *Cryptococcus gattii* population develops clonal outbreak
573 clusters through both sexual macroevolution and asexual microevolution. mBio
574 5**:** e01494-01414.
575 Boekhout, T., B. Theelen, M. Diaz, J. W. Fell, W. C. J. Hop *et al.*, 2001 Hybrid genotypes
576 in the pathogenic yeast *Cryptococcus neoformans*. Microbiology 147**:** 891-907.
577 Bovers, M., F. Hagen, E. E. Kurumae, H. L. Hoogveld, F. Dromer *et al.*, 2008 AIDS patient
578 death caused by novel *Cryptococcus neoformans* x *C. gattii* hybrid. Emerg.
579 Infect. Dis. 14**:** 1105-1108.
580 Boyce, K. J., Y. Wang, S. Verma, V. P. S. Shakya, C. Xue *et al.*, 2017 Mismatch repair of
581 DNA replication errors contributes to microevolution in the pathogenic fungus
582 *Cryptococcus neoformans*. mBio 8**:** e00595-00517.
583 Bui, T., X. Lin, R. Malik, J. Heitman and D. Carter, 2008 Isolates from *Cryptococcus*
584 *neoformans* from infected animals reveal genetics exchange in unisexual, α
585 mating type population. Eukaryot. Cell 7**:** 1771-1780.
586 Casadevall, A., J. B. Freij, C. Hann-Soden and J. Taylor, 2017 Continental drift and
587 speciation of the *Cryptococcus neoformans* and *Cryptococcus gattii* species
588 complexes. mSphere 2**:** e00103-00117.

589 Casadevall, A., J. Mukherjee, S. J. N. Devi, R. Schneerson, J. B. Robbins *et al.*, 1992
590 Antibodies elicited by a *Cryptococcus neoformans*-tetanus toxoid conjugate
591 vaccine have the same specificity as those elicited in infection. The Journal of
592 Infectious Diseases 165**:** 1086-1093.
593 Cuomo, C. A., J. Rhodes and C. A. Desjardins, 2018 Advances in *Cryptococcus* genomics:
594 insights into the evolution of pathogenesis. Mem. Inst. Oswaldo Cruz 113.
595 Dal Pupo, H. D., B. A. G. Sena, F. C. G. Reis, L. Machado, S. T. Fortes *et al.*, 2019
596 Polysaccharide diversity in VNI isolates of *Cryptococcus neoformans* from
597 Roraima, Northern Brazil. Fungal Biology 123**:** 699-708.
598 Dambuza, I. M., T. Drake, A. Chapuis, X. Zhou, J. Correia *et al.*, 2018 The *Cryptococcus*
599 *neoformans* Titan cell is an inducible and regulated morphotype underlying
600 pathogenesis. PLoS Pathog. 14**:** e1006978.
601 de Sousa, H. R., G. P. de Oliveira, S. de Oliveira Frazão, K. C. de Melo Gorgonha, C. P.
602 Rosa *et al.*, 2020 Faster *Cryptococcus* melanization increases virulence in
603 experimental and human cryptococcosis. bioRxiv**:** 2020.2007.2029.222794.
604 Desjardins, C. A., C. Giamberardino, S. M. Sykes, C.-H. Yu, J. L. Tenor *et al.*, 2017
605 Population genomics and the evolution of virulence in the fungal pathogen
606 *Cryptococcus neoformans*. Genome Res. 27**:** 1207-1219.
607 Engelthaler, D. M., N. D. Hicks, J. D. Gillece, C. C. Roe, J. M. Schupp *et al.*, 2014
608 *Cryptococcus gattii* in North American Pacific Northwest: Whole-Population
609 Genome Analysis Provides Insights into Species Evolution and Dispersal. mBio
610 5**:** e01464-01414.
611 Ergin, Ç., M. Şengül, L. Aksoy, A. Döğen, S. Sun *et al.*, 2019 *Cryptococcus neoformans*
612 recovered from olive trees (*Olea europaea*) in Turkey reveal allopatry with
613 African and South American lineages. Frontiers in Cellular and Infection
614 Microbiology 9.
615 Farrer, R. A., M. Chang, M. J. Davis, L. van Dorp, D.-H. Yang *et al.*, 2019 A new lineage
616 of *Cryptococcus gattii* (VGV) discovered in the central Zambezian Miombo
617 Woodlands. mBio 10**:** e02306-02319.
618 Ferreira-Paim, K., L. Andrade-Silva, F. M. Fonseca, T. B. Ferreira, D. J. Mora *et al.*, 2017
619 MLST-based population genetic analysis in a global context reveals clonality
620 amongst *Cryptococcus neoformans* var. *grubii* VNI isolates from HIV patients in
621 Southeastern Brazil. PLOS Neglected Tropical Diseases 11**:** e0005223.
622 Foster, P. L., 2006 Methods for determining spontaneous mutation rates. Methods in
623 enzymology 409**:** 195-213.
624 Garcia-Hermoso, D., G. Janbon and F. Dromer, 1999 Epidemiological evidence for
625 dormant *Cryptococcus neoformans* infection. Journal of Clinical Microbiology
626 37**:** 3204-3209.
627 Gillet-Markowska, A., G. Louvel and G. Fischer, 2015 *bz-rates*: A Web Tool to Estimate
628 Mutation Rates from Fluctuation Analysis. G3: Genes|Genomes|Genetics 5**:**
629 2323.
630 Gonzalez-Hilarion, S., D. Paulet, K.-T. Lee, C.-C. Hon, P. Lechat *et al.*, 2016 Intron
631 retention-dependent gene regulation in *Cryptococcus neoformans*. Sci. Rep. 6**:**
632 32252.
633 Gou, L., J. S. Bloom and L. Kruglyak, 2019 The genetic basis of mutation rate variation
634 in yeast. Genetics 211**:** 731-740.

635 Gröhs Ferrareze, P. A., C. Maufrais, R. Silva Araujo Streit, S. J. Priest, C. A. Cuomo *et al.*,
636 2021 Application of an optimized annotation pipeline to the *Cryptococcus*
637 *deuterogattii* genome reveals dynamic primary metabolic gene clusters and
638 genomic impact of RNAi loss. G3 (Bethesda) 11.
639 Guindon, S., J.-F. Dufayard, V. Lefort, M. Anisimova, W. Hordijk *et al.*, 2010 New
640 algorithms and methods to estimate maximum-likelihood phylogenies:
641 assessing the performance of PhyML 3.0. Systematic Biology 59**:** 307-321.
642 Hagen, F., P. C. Ceresini, I. Polacheck, H. Ma, F. v. Nieuwerburgh *et al.*, 2013 Ancient
643 dispersal of the human fungal pathogen *Cryptococcus gattii* from the Amazon
644 rainforest. PLOS ONE 8**:** e71148.
645 Hagen, F., K. Khayhan, B. Theelen, A. Kolecka, I. Polacheck *et al.*, 2015 Recognition of
646 seven species in the *Cryptococcus gattii*/*Cryptococcus neoformans* species
647 complex. Fungal Genet. Biol. 78**:** 16-48.
648 Hommel, B., L. Mukaremera, R. J. B. Cordero, C. Coelho, C. A. Desjardins *et al.*, 2018
649 Titan cells formation in *Cryptococcus neoformans* is finely tuned by
650 environmental conditions and modulated by positive and negative genetic
651 regulators. PLoS Pathog. 14**:** e1006982.
652 Institute, C. L. S., 2017 Reference method for broth dilution antifungal susceptibility
653 testing of yeasts; approved standard, document document M27-A3 in *National*
654 *Committee for Clinical Laboratory Standards*.
655 Janbon, G., K. L. Ormerod, D. Paulet, E. J. Byrnes III, G. Chatterjee *et al.*, 2014 Analysis
656 of the genome and transcriptome of *Cryptococcus neoformans* var. *grubii*
657 reveals complex RNA expression and microevolution leading to virulence
658 attenuation. PLoS Genet. 10**:** e1004261.
659 Janbon, G., J. Quintin, F. Lanternier and C. d'Enfert, 2019 Studying fungal pathogens of
660 humans and fungal infections: fungal diversity and diversity of approaches.
661 Genes & Immunity 20**:** 403-414.
662 Johnston, S. A., K. Voelz and R. C. May, 2016 *Cryptococcus neoformans*
663 thermotolerance to avian body temperature is sufficient for extracellular
664 growth but not intracellular survival in macrophages. Sci. Rep. 6**:** 20977.
665 Kidd, S. E., F. Hagen, R. L. Tscharke, M. Huynh, K. H. Bartlett *et al.*, 2004 A rare
666 genotype of *Cryptococcus gattii* caused the cryptococcosis outbreak on
667 Vancouver Island (British Columbia, Canada). Proc. Natl. Acad. Sci. U.S.A. 101**:**
668 17258-17263.
669 Kwon-Chung, K. J., and J. E. Bennett, 1978 Distribution of a and α mating types of
670 *Cryptococcus neoformans* among natural and clinical isolates. Am. J. Epidemiol.
671 108**:** 337-340.
672 Kwon-Chung, K. J., J. A. Fraser, T. L. Doering, Z. Wang, G. Janbon *et al.*, 2014
673 *Cryptococcus neoformans* and *Cryptococcus gattii*, the etiologic agents of
674 cryptococcosis. Cold Spring Harb Perspect Med 4**:** a019760.
675 Li, H., 2018 Minimap2: pairwise alignment for nucleotide sequences. Bioinformatics
676 34**:** 3094-3100.
677 Li, H., B. Handsaker, A. Wysoker, T. Fennell, J. Ruan *et al.*, 2009 The Sequence
678 Alignment/Map format and SAMtools. Bioinformatics (Oxford, England) 25**:**
679 2078-2079.
680 Lin, X., and J. Heitman, 2006 The biology of the *Cryptococcus neoformans* species
681 complex. Ann. Rev. Microbiol. 60**:** 69-105.

682 Lin, X., S. Patel, A. P. Litvintseva, A. Floyd, T. G. Mitchell *et al.*, 2009 Diploids in the
683 *Cryptococcus neoformans* serotype A population homozygous for the alpha
684 mating type originate via unisexual mating. PLoS Pathog. 5**:** e1000283.
685 Litvintseva, A. P., I. Carbone, J. Rossouw, R. Thakur, N. P. Govender *et al.*, 2011
686 Evidence that the human pathogenic fungus *Cryptococcus neoformans* var.
687 grubii may have evolved in Africa. PloS One 6**:** e19688.
688 Litvintseva, A. P., L. Kestenbaum, R. Vilgalys and T. G. Mitchell, 2005 Comparative
689 analysis of environmental and clinical populations of *Cryptococcus neoformans*.
690 Journal of Clinical Microbiology 43**:** 556-564.
691 Litvintseva, A. P., X. Lin, I. Templeton, J. Heitman and T. G. Mitchell, 2007 Many
692 globally isolated AD hybrid strains of *Cryptococcus neoformans* originated in
693 Africa. PLoS Pathog. 3**:** e114.
694 Litvintseva, A. P., R. E. Marra, K. Nielsen, J. Heitman, R. Vilgalys *et al.*, 2003 Evidence of
695 sexual recombination among *Cryptococcus neoformans* serotype A isolates in
696 sub-Saharan Africa. Eukaryot. Cell 2**:** 1162-1168.
697 Litvintseva, A. P., and T. G. Mitchell, 2012 Population genetic analyses reveal the
698 African origin and strain variation of *Cryptococcus neoformans* var. *grubii*. PLoS
699 Pathog. 2012**:** e1002495.
700 Loftus, B., E. Fung, P. Roncaglia, D. Rowley, P. Amedeo *et al.*, 2005 The genome and
701 transcriptome of *Cryptococcus neoformans*, a basidiomycetous fungal pathogen
702 of humans. Science 307**:** 1321-1324.
703 Matsumoto, M. T., A. M. Fusco-Almeida, L. C. Baeza, M. d. S. C. Melhem and M. J. S.
704 Medes-Giannini, 2007 Genotyping, serotyping and determination of mating-
705 type of *Cryptococcus neoformans* clinical isolates from São Paulo State, Brazil.
706 Revista do Instituto de Medicina Tropical de São Paulo 49**:** 41-47.
707 Meyer, W., D. M. Aanensen, T. Boekhout, M. Cogliati, M. R. Diaz *et al.*, 2009a
708 Consensus multi-locus sequence typing scheme for *Cryptococcus neoformans*
709 and *Cryptococcus gattii*. Med. Mycol. 47**:** 561-570.
710 Meyer, W., D. M. Aanensen, T. Boekhout, M. Cogliati, M. R. Diaz *et al.*, 2009b
711 Consensus multi-locus sequence typing scheme for *Cryptococcus neoformans*
712 and *Cryptococcus gattii*. Med. Mycol. 57**:** 561-570.
713 Prum, R. O., J. S. Berv, A. Dornburg, D. J. Field, J. P. Townsend *et al.*, 2015 A
714 comprehensive phylogeny of birds (Aves) using targeted next-generation DNA
715 sequencing. Nature 526**:** 569-573.
716 Raj, A., M. Stephens and J. K. Pritchard, 2014 fastSTRUCTURE: Variational Inference of
717 Population Structure in Large SNP Data Sets. Genetics 197**:** 573.
718 Rajasingham, R., R. M. Smith, B. J. Park, J. N. Jarvis, N. P. Govender *et al.*, 2017 Global
719 burden of disease of HIV-associated cryptococcal meningitis: an updated
720 analysis. The Lancet Infectious Diseases 17**:** 873-881.
721 Rhodes, J., M. A. Beale, M. Vanhove, J. N. Jarvis, S. Kannambath *et al.*, 2017a A
722 population genomics approach to assessing the genetic basis of within-host
723 microevolution underlying recurrent cryptococcal meningitis infection. G3:
724 Genes|Genomes|Genetics 7**:** 1165.
725 Rhodes, J., C. A. Desjardins, S. M. Sykes, M. A. Beale, M. Vanhove *et al.*, 2017b Tracing
726 genetic exchange and biogeography of *Cryptococcus neoformans* var. *grubii* at
727 the global population level. Genetics**:** 10.1534/genetics.1117.203836.

728 Ruma, P., S. C. A. Chen, T. C. Sorrel and A. G. Brownlee, 1996 Characterization of
729 *Cryptococcus neoformans* by random DNA amplification. Letters in Applied
730 Microbiology 23**:** 312-316.
731 Silva, D. C., M. A. Martins, M. W. Szeszs, L. X. Bonfietti, D. Matos *et al.*, 2012
732 Susceptibility to antifungal agents and genotypes of Brazilian clinical and
733 environmental *Cryptococcus gattii* strains. Diagnostic Microbiology and
734 Infectious Disease 72**:** 332-339.
735 Souto, A. C. P., L. X. Bonfietti, K. Ferreira-Paim, L. Trilles, M. Martins *et al.*, 2016
736 Population genetic analysis reveals a high genetic diversity in the Brazilian
737 *Cryptococcus gattii* VGII population and shifts the global origin from the
738 amazon rainforest to the semi-arid desert in the Northeast of Brazil. PLoS
739 neglected tropical diseases 10**:** e0004885-e0004885.
740 Trevijano-Contador, N., H. C. de Oliveira, R. García-Rodas, S. A. Rossi, I. Llorente *et al.*,
741 2018 *Cryptococcus neoformans* can form titan-like cells in vitro in response to
742 multiple signals. PLoS Pathog. 14**:** e1007007.
743 Vanhove, M., M. A. Beale, J. Rhodes, D. Chanda, S. Lakhi *et al.*, 2017 Genomic
744 epidemiology of *Cryptococcus* yeasts identifies adaptation to environmental
745 niches underpinning infection across an African HIV/AIDS cohort. Mol. Ecol. 26**:**
746 1991-2005.
747 Vilas-Bôas, A. M., L. E. Andrade-Silva, K. Ferreira-Paim, D. J. Mora, T. B. Ferreira *et al.*,
748 2020 High genetic variability of clinical and environmental *Cryptococcus gattii*
749 isolates from Brazil. Med. Mycol. 58**:** 1126-1137.
750 Yadav, V., S. Sun, R. B. Billmyre, B. C. Thimmappa, T. Shea *et al.*, 2018 RNAi is a critical
751 determinant of centromere evolution in closely related fungi. Proc. Natl. Acad.
752 Sci. U.S.A. 115**:** 3108.
753 Zaragoza, O., and K. Nielsen, 2013 Titan cells in *Cryptococcus neoformans*: Cells with a
754 giant impact. Current Opinion in Microbiology 16**:** 409-413.
755